Optimzition of the Bi2O3Cu synthesis process using response surface methodology as a tetracycline photodegradation agent

by Heri Sutanto

Submission date: 26-Feb-2023 02:02PM (UTC+0700)
Submission ID: 2023108987
File name: urface_methodology_as_a_tetracycline_photodegradation_agent.pdf (8.06M)
Word count: 8568
Character count: 44526

Results in Engineering 16 (2022) 100521

Contents lists available at ScienceDirect

Results in Engineering

journal homepage: www.sciencedirect.com/journal/results-in-engineering

Optimization of the Bi_2O_3/Cu synthesis process using response surface methodology as a tetracycline photodegradation agent

Fatkhiyatus Sa'adah [a], Heri Sutanto [b,c,*], Hadiyanto [a]

[a] Department of Environmental Science, Postgraduate School, Diponegoro University, Semarang, Indonesia
[b] Department of Physics, Faculty of Science and Mathematics, Diponegoro University, Semarang, Indonesia
[c] Smart Materials Research Center (SMARC), Diponegoro University, Semarang, Indonesia

ARTICLE INFO

Keywords:
Bismuth oxide
Photodegradation
Microwave-precipitation
Tetracycline

ABSTRACT

This study examined the ability of the photocatalyst material bismuth oxide doped Cu (Bi_2O_3/Cu) in degrading Tetracycline. Bi_2O_3/Cu material synthesis has been successfully carried out by the microwave-assisted precipitation method. The synthesis process was carried out by variations in Cu concentration, power, and synthesis time. Optimization was carried out on synthesis variations with Response Surface Methodology (RSM) using central composite design (CCD) techniques. The response studied was the value of degradation efficiency (Ef). The best results obtained at R19 with a concentration composition of Cu 6%, power of 600 W and synthesis time of 60 min resulted in a degradation efficiency value against Tetracycline of 61.09%. XRD characterization results show that the material formed was phase α-Bi_2O_3 and Garhadite ($Cu_2H_3NO_6$) with compositions of 71.9% and 28.1%. FWHM values obtained are 0.2636 and 0.2877, respectively. The resulting crystal size was 31.23874 nm. The results of this characterization proven that Cu metal has been successfully doped in Bi_2O_3 material.

1. Introduction

The increment of drugs consumption in public causes pollution and a decrement in environmental quality when released directly from the pharmaceutical industry, hospitals, and other medical installations [1]. The risk was increasing dangerously since the disposal of drug waste has not been managed properly till now. One of the pollutants that still pollutes the environment even after passing a series of Wastewater Treatment Plants (WWTP) is pharmaceutical waste or drug waste [2]. One of the drugs widely consumed by people is antibiotics [3].

Some antibiotics have been detected in wastewater [4,5], sludge [6, 7], groundwater [8], surface water [9], sediment [10], and soil [11]. The biotechnological approach that is widely applied by WWTP has not been able to degrade antibiotics effectively but only transfers pollutants from one phase to another and increases the incidence of microbial resistance to antibiotics trapped in physical filters [12].

Tetracycline (TC) is a main class of antibiotics that are often used in hospital medicine due to their broad antibacterial activity against a wide range of gram-positive and gram-negative bacteria [13]. After treatment, more than 70% of TC is released in an active form into the environment. In recent years, the presence of TC in surface water and groundwater is up to 20 mg/L with half of 139 rivers that are being surveyed in the US are have been detected the presence of TC [14]. The reported average concentration of TC in US surface water is 1.34 mg/L [15].

Several techniques for TC degradation have been reported, but the efficiency in TC removal was still relatively low [16]. Among the good TC removal technologies that involve physical, chemical, and biological processes to remove TC are adsorption methods [17], coagulation [18], membrane separation [19], aerobic degradation, and anaerobic degradation [20].

Researchers are currently developing a TC degradation technique using the Advance Oxidation Process (AOPs) method [21–25]. The AOPs method is a method of utilizing the oxidation reaction process. One of the materials that can be used in this technique is photocatalyst material. The material that has been commonly used as a photocatalyst agent is Titanium Dioxide (TiO_2) [26]. TiO_2 has been commonly used in waste degrading applications, including for pharmaceutical waste [27,28]. The main problem in TiO_2 employment is the large bandgap hence the photocatalytic process is only effective under UV light [29].

Bismuth-based oxide materials such as Bi_2O_3, $BiPO_4$, $BiVO_4$, Bi_2WO_6 are strong candidates that can replace TiO_2 due to their excellent photocatalytic activity in the decomposition of organic compounds, water separation, and NO reduction [30–32]. Several previous studies have

* Corresponding author. Department of Physics, Faculty of Science and Mathematics, Diponegoro University, Semarang, Indonesia.
E-mail address: herisutanto@live.undip.ac.id (H. Sutanto).

https://doi.org/10.1016/j.rineng.2022.100521
Received 11 May 2022; Received in revised form 26 June 2022; Accepted 26 June 2022
Available online 9 July 2022

also shown that bismuth oxide has been able to degrade antibiotics [33] such as sulfamethoxazole [31], amoxicillin, tetracycline, and ciprofloxacin [34].

From several types, Bismuth Oxide (Bi_2O_3) has been proven to work optimally under visible-light with a bandgap of 2.58–2.85 eV Bi_2O_3 material was increasingly interesting to be studied in more depth because it has magnetic properties, namely the internal field and longitudinal magnetoelectric effect. The property of Bi_2O_3 is highly determined by the structure of the crystalline phase. The photocatalytic activity of Bi_2O_3 is highly dependent on its crystalline structure and morphology. In photocatalyst applications, Bi_2O_3 was relevant for use in the α and β phases. Thus, controlled preparation of Bi_2O_3 with a certain crystalline phase, especially in photocatalysis is very important [35].

To get a suitable Bi_2O_3 in the application of photocatalyst material, it is necessary to determine the right synthesis method. Recently, doping of photocatalysts with metal atoms has become a popular method to improve photocatalyst performance [36,37]. The addition of metals such as copper (Cu) is possible to reduce the energy bandgap of the semiconductor photocatalyst hence producing a wider light response and increasing its photocatalytic activity [38].

The synthesis of photocatalyst materials can be carried out by several methods, such as spray pyrolysis, electrospinning, hydrothermal, precipitation, and sol-gel. In general, these methods require quite high production costs, thus it is necessary to consider other more efficient methods. The precipitation method is an effective method for obtaining a precipitate without changing the composition of the compound and the composition of the material [39]. The development of a new method using microwave irradiation is a promising alternative. This method uses the principle of vibrating compound bonds using microwaves generated by a magnetron. Microwave irradiation is the right choice since it is easy to fabricate and the cost expended is lower than other methods, and is a one-step synthesis [40].

Until now, the optimization of the Bi_2O_3 synthesis with the influence of several material compositions andsynthesis process has not been optimally carried out. Due to the complexity and various factors that affect the efficiency value of the degradation factor, it is difficult to apply several influencing factors. In this research, the Bi_2O_3 semiconductor will be added with Cu metal (Bi_2O_3/Cu) with the microwave-assisted precipitation method. This experiment can increase the speed of electron-hole pair separation by acting as a shallow trap and reducing the speed of electron-hole recombination in Bi_2O_3/Cu materials. The synthesis process was carried out by optimization method using Response Surface Methodology (RSM) with Central Composite Design (CCD) technique to obtain optimal TC degradation efficiency values. Finally, the authors hope to be able to produce innovative materials that are effective in degrading TC.

2. Methods

2.1. Tools and materials

The materials used in this study include Bismuth Nitrate Bi $(NO_3)_3.5H_2O$ (Merck KgaA), Nitric Acid (HNO_3) 65% (Merck KgaA), Sodium Hydroxide (NaOH) 1 M, Copper (II) Nitrate $(Cu(NO_3)_3{\cdot}3H_2O$ (Merck KgaA), Aquades, and Tetracycline Antibiotics (Novapharine, Pharmaceutical Industries).

The tools used include a microwave reactor (Samsung MS28J5255UB, frequency 50 Hz, power 100–1000 Watt), digital scale (Ohauss PX224/E, maximum weight 220 g, accuracy 0.1 mg), spatula, mortar, cup, beaker, measuring cup, centrifuge (SCILOGEX DM0412, frequency 50 Hz, speed 300–450 rpm), Hotplate Magnetic Stirrer (SCILOGEX MSH280, speed 100–1500 rpm, 25-280 °C), Ultra turrax (IKA Disperser T18, frequency 50 Hz, speed 3000–25,000 rpm), and UV-C lamp.

2.2. Research stages

This research was conducted in several stages. The first stage begins with the synthesis of Bi_2O_3/Cu photocatalyst material using the microwave-assisted precipitation method. After the synthesis process, the photocatalyst material is then characterized in order to determine the optical characteristics of the resulting material. . In the application stage, Bi_2O_3/Cu photocatalyst material was applied to degrade tetracycline.

2.3. Material synthesis

Bi_2O_3/Cu material was synthesized with the precipitation method using the microwave. Bismuth nitrate 0.5 g and Copper nitrate with different mass (0.00318, 0.01, 0.02, 0.03, and 0.03682 g) were added to 50 mL nitric acid 5% (1 moL/l). The solution was then homogenized using a stirrer (500 rpm) for 10 min at room temperature. The homogeneous solution was then added with 250 mL of sodium hydroxide (1 moL/l) and stirred with a stirrer for 2 h. The results of stirring are then precipitated and the precipitate was separated and heated on a hotplate for 2 h at 120 °C to become Bi_2O_3/Cu powder. The powder was then fed into a microwave reactor with a predetermined power (180, 300, 450, 600, and 850 W) and synthesis time (20, 30, 45, 60, and 70 min). The schematic of the synthesis of Bi_2O_3/Cu material can be seen in Fig. 1.

The research design used to optimize the synthesis process was Central Composite Design (CCD) using Design-Expert 10 software. The variables evaluated were Cu concentration (0.636, 2, 4, 6, and 7.364) (A, %), power (180, 300, 450, 600 and 850) (B, Watt) and synthesis time (20, 30, 45, 60 and 70) (C, min). The observed response is the degradation efficiency (Ef, %). Variables and research levels are presented in Table 1.

2.4. Material characterization

Analysis of the structure and crystalline phase of Bi_2O_3/Cu powder was carried out using XRD brand Shimadzu XRD 6100/7000 at the Integrated Laboratory of Diponegoro University (UNDIP). The X-ray wavelength used is 1.54016 Å. Data retrieval is carried out every 0.02°. The crystal size of Bi_2O_3/Cu was calculated using the Debbye-Scherrer equation [41].

$$Ds = \frac{k\,\lambda}{\beta \cos\theta} \tag{1}$$

with Ds is the crystallyte size (nm), $\lambda = 1.5406\ nm$ is the wavelength of X-rays, $k = 0.9$ is the Scherrer constant, β is the Full Width and Half Maximum or FWHM (in radians), and θ is the Bragg angle of diffraction or peak position (in radians)

UV–Vis characterization was done to find out the absorption spectrum which was then processed using the Tauc plot technique to get the value of the energy bandgap (Eg) of Bi_2O_3/Cu material. Analysis of morphology and material content is obtained from Scanning Electron Microscopy-Energy Dispersive of X-Ray (SEM-EDX) characterization data.

2.5. Tetracycline degradation

The degradation process begins with making a TC solution with a concentration of 1000 ppm in distilled water. This solution was manufactured by a procedure once performed by Tanveer et al. [3]. A total of 1 g of >98% impurity TC powder was dissolved in aqueous until it reached a volume of 1 L. Then, the solution was stirred until homogeneous. 100 mL of TC solution was taken and added with Bi_2O_3/Cu which had been produced in the experimental design in Table 1. The solution was then put into a degradator box that had been installed with a UV lamp. The degradation process was carried out under UV light in a span

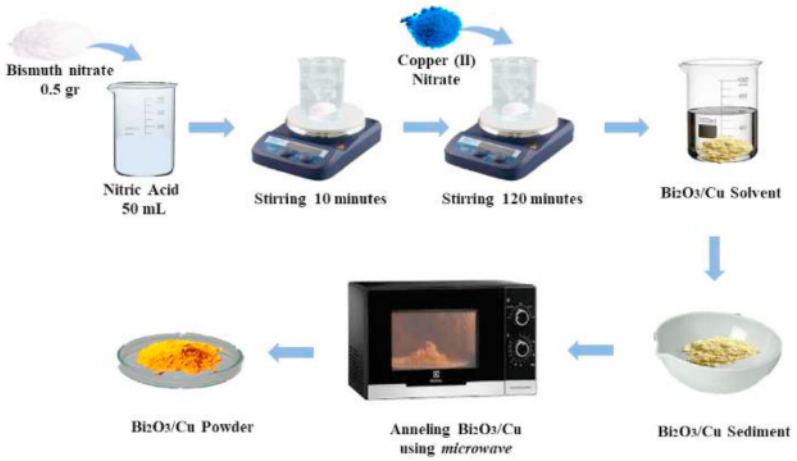

Fig. 1. Process of synthesis Bi_2O_3/Cu.

Table 1
Variable and level experiment using CCD.

Symbol	Variable	Unit	Level				
			-alfa	−1	0	+1	+alfa
A	Cu Concentration	%	0.636	2	4	6	7.364
B	Power	Watt	180	300	450	600	850
C	Time	Minutes	20	30	45	60	70

of 120 min. The application process is represented in Fig. 2.

The degradation results will be analyzed using a UV–vis spectrophotometer instrument. Photometric techniques can calculate degradation efficiency through data on concentration values before and after Tetracycline degradation. Photocatalyst efficiency (Ef) is calculated using the following equation:

$$Ef(\%) = \left(1 - \frac{C_t}{C_0}\right) \times 100\% \quad (2)$$

with C_0 and C_t are the initial and final concentrations of liquid, and Ef is the degradation efficiency (%).

3. Result and discussion

3.1. Synthesis of Bi_2O_3/Cu material

Bi_2O_3/Cu has been successfully synthesized using the microwave-assisted precipitation method. The synthesis was carried out for 20 samples, namely samples R1 to R20 which were adjusted to the research design using Response Surface Methodology. The employment of the Central Composite Design technique was chosen by providing 3 factors and 1 response, namely the efficiency of material degradation.

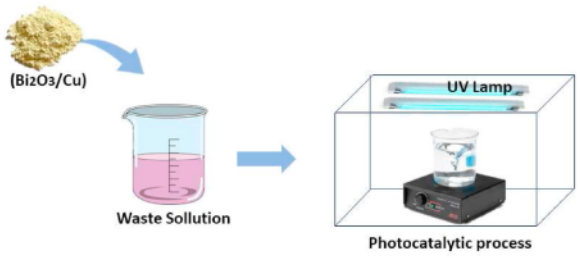

Fig. 2. Tetracycline degradation by Bi_2O_3/Cu.

The synthesis process produces a green Bi_2O_3/Cu powder. The addition of Cu to Bi_2O_3 material causes color differences as shown in Fig. 3. Color changes occur when the dissolved $Cu(NO_3)_3{\cdot}3H_2O$ is being blue and mixed with the yellow $Bi(NO_3)_3{\cdot}5H_2O$ hence the color will shift in the opposite direction of the substance to produce a green color. All Bi_2O_3/Cu samples produced with different compositions of Cu concentration, power, and synthesis time resulted in a uniform green color. The resulting green color increased as the concentration of Cu was added. This color shift occurs due to changes in conditions at the reaction equilibrium. This is in accordance with Le Chatelier's principle which states that if colored ions are added to a reaction, the compound formed will become darker [42].

To confirm the success of the synthesis process, characterization was carried out including the crystalline phase of the material, also the structure and size of the material.

3.2. Data analysis and model evaluation with RSM

The experimental design of CCD statistics in this study was used to optimize 3 factors, namely Cu concentration, power, and synthesis time. The resulting response is a tetracycline degradation efficiency value. The CCD technique is a design of 2 k factorial or partial factorial consisting of 3 levels, namely −1, 0, and +1, also the CCD level that expanded with the addition of -alpha and +alpha. CCD allows a larger number of levels without running every combination of trials and results in more trials [43]. The CCD model in this experiment has a total of 20 experimental runs. The experimental data obtained were then evaluated using statistical analysis of variance (ANOVA) and p-value (probability).

The result data, namely the value of the degradation efficiency of the Bi_2O_3/Cu material against tetracycline is shown in Table 2. The actual degradation efficiency value was obtained from experiments that have been calculated using Eq. (2), while the predicted value is obtained from calculations using *Design-Expert* software.

The value of the degradation efficiency yielded from each experimental design shown a different value. Differences in composition between factors of Cu concentration, power, and time of synthesis will result in different degradation efficiency values. The highest degradation efficiency value was obtained at R19 of 61.09% with variations of Cu concentration of 6%, 600 W of power, and 60 min of synthesis time. The lowest response was at R5 with a combination of 2% Cu

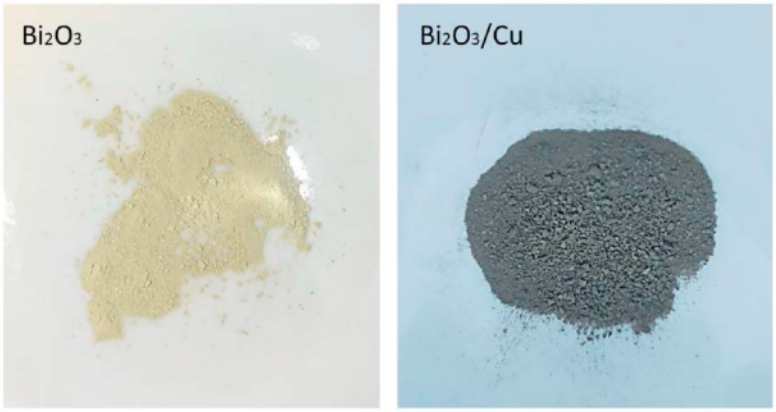

Fig. 3. Differences between Bi_2O_3 and Bi_2O_3/Cu synthesis results.

Table 2
Degradation efficiency response data of Bi_2O_3/Cu material.

Run	Factor			Actual Factor			Degradation Efficiency	
	A	B	C	Cu Concentration (%)	Power (Watt)	Time (Minutes)	Actual (%)	Prediction (%)
R1	0	0	+alfa	4	450	70	58.47	55.80
R2	−1	−1	+1	2	300	60	32.00	33.06
R3	0	0	0	4	450	45	41.60	49.52
R4	−1	+1	+1	2	600	60	40.45	43.74
R5	−1	−1	−1	2	300	30	21.28	20.82
R6	0	0	0	4	450	45	45.84	49.52
R7	−1	+1	−1	2	600	30	32.05	35.94
R8	0	0	0	4	450	45	47.48	49.52
R9	0	0	0	4	450	45	50.27	49.52
R10	-alfa	0	0	0.636	450	45	30.80	27.59
R11	0	0	0	4	450	45	56.32	49.52
R12	0	0	0	4	450	45	58.91	49.52
R13	+1	−1	−1	6	300	30	27.55	27.20
R14	0	0	-alfa	4	450	20	29.24	27.68
R15	+alfa	0	0	7.364	450	45	51.35	50.40
R16	+1	−1	+1	6	300	60	54.09	53.14
R17	0	+alfa	0	4	850	45	50.07	47.09
R18	0	-alfa	0	4	180	45	25.56	28.46
R19	+1	+1	+1	6	600	60	61.09	64.49
R20	+1	+1	−1	6	600	30	41.11	42.99

concentration, 300 power and 30 min of synthesis time which resulted in a degradation efficiency value of 21.28%. Differences in response values in each study design show that differences in concentration composition, power and synthesis time will produce different response values. From this optimization process, it was concluded that the R19 sample as the best sample would then be characterized to find out its optical properties.

The Table 2 shown that the actual and predicted degradation efficiency values do not show a significant difference. The comparison of actual and predicted values shown that the resulting model is appropriate to describe the actual conditions and yields a high accuracy value. This is evidenced by the inaccuracy test (lack of fit) of the actual degradation efficiency response and predictions shown in the Table 3.

The lack of fit test aims to determine the suitability or inaccuracy of the model in describing existing data. The selected model with the status "suggested" with a *p-value* (Prob > F) of 0.8374 or 83.74% which means that the *p-value* > 5% so that the model has a lack of fit with the degree of significance used, which is 0.05. If the *p-value* of the data exceeds the alpha level (0.05), the model is significant and has no inaccuracy (lack of fit) in describing the data. So that actual data and predictions are expressed significantly [44].

Table 3
Test results of lack of fit test of degradation efficiency response.

Source	Sum of Squares	df	Mean Square	F value	P- value Prob > F	
Linear	674.61	11	61.33	1.44	0.3629	
2Fl	570.69	8	71.34	1.67	0.2966	
Quadratic	83.38	5	16.68	0.39	0.8374	
Cubic	0	0				*Aliased*
Pure Error	213.59	5	42.72			

Statistical analysis for the degradation efficiency response shows that the selected model is quadratic. The selection of this model is determined based on the analysis of the summary statistics model in the following Table 4.

Model selection is determined based on the standard deviation value, R-squared, Adjusted R-squared, Predicted R-squares, and PRESS (Prediction residual error sum of a square) Values Selected quadratic models with consecutive values of 5.45, 0.8985, 0.8071, and 0.5191. The quadratic model was chosen because it has an R-squared value close to 1. The R-squared value obtained is 0.8985 which means that the

Table 4
Summary statistics model.

Source	Std. Dev	R-squared	Adjusted R-squared	Predicted R-squared	PRESS	
Linear	7.45	0.6964	0.6395	0.5735	1247.84	
2Fl	7.77	0.7319	0.6082	0.4088	1729.46	
Quadratic	5.45	0.8985	0.8071	0.5191	1406.91	Suggested
Cubic	6.54	0.9270	0.7726		+	Aliased

experimental factor exerts an influence of 89.85% on the response value. An independent variable (factor) is said to influence on the response if it has an R-squared value of ≥80%. The Adjusted R-squared value obtained on this model is also close to 1 which is 0.8071 which means it indicates a high model fit [45]. The standard deviation value generated in the selected model is the lowest. The lower the standard deviation value indicates the resulting uniformity value the higher. A low PRESS value also indicates that the error rate of data prediction on the program is getting smaller. So based on the summary statistical model the quadratic model is selected with the status of "suggested".

In addition, the selection of models is also determined from the values of p-value, f-value, and lack of fit. The quadratic model was found to be significant when it had a p-value of <0.05. F-value is used to estimate the statistical significance of all factors in a polynomial equation with a confidence level of 95%. The greater the f-value, the smaller the p-value, and the more significant the result. Lack of fit is obtained from replication at the central point which aims to find out experimental errors. The lack of fit value obtained is p-value 0.8374 with a status of "not significant". These results show that the experiment has been appropriately used and does not differ much from the resulting model. The f-value generated in this model is 9.83 and the p-value is 0.0174 which indicates that this model is statistically significant as seen in Table 5.

Based on Table 5, the selected models are quadratic models with a sum of squares of 2628.56, mean square 292.06, F value of 9.83, and p-value of 0.0007. Quadratic models with a p-value of <0.05 indicate that the model can present data well and influence the degradation efficiency response. The concentration factor (A) has a sum of squares of 628.15, mean squares of 628.15, F-value of 21.15, and p-value of 0.0010. The concentration factor has a p-value of <0.05, which indicates that the concentration factor can present the data well and influences the degradation efficiency value. Power factor (B) has a sum of square value of 672.90, mean squares 672.90, F-value 22.66, and p-value 0.0008. The resulting p-value <0.05 indicates that the power factor influences the degradation efficiency value. The synthesis time factor (C) has a sum of squares value of 964.73, mean squares 964.73, F-value 32.49, and p-value 0.0002. The resulting p-value <0.05 indicates that the time factor can present the data well and influence the resulting degradation efficiency value.

The interaction between factors A^2, B^2, and C^2 also has a p-value of <0.05. The resulting p-value of 0.0283, 0.0076, and 0.0086, respectively, indicate that the square of the factor also influences the degradation efficiency value. P-value <0.05 can be interpreted to mean that the model and factor have a noticeable influence on the degradation efficiency response. Lack of fit in the table shows a caption "not significant" because the p-value> 0.05. This result indicates that the selected model has appropriately been used, and the error has no effect on the model [46].

The degradation efficiency response equation generated in the quadratic model is as follows:

$$\text{Degradation efficiency} = 49.52 + 6.78A + 6.62B + 8.44C + 0.17AB + 3.43AC - 1.11BCE - 3.72A^2 - 2.82B^2 - 2.80C^2$$

with Ef is the degradation efficiency response value (%), A is the Cu Concentration factor (%), B is the power factor (watt) and the C is synthesis time factor (minutes).

This equation was used to determine the value of the degradation efficiency response obtained if different concentrations, power, and synthesis times are used. Based on the equation, the most influential variable for ef response was the time factor with a coefficient value of 8.44. The + sign means that each 1-point increase will have an effect of 8.44 on the degradation efficiency value.

To find out the influence between variables on the response will be presented using a graph of the contours of the plot and the surface of the response. The interaction between the concentration and power factors were represented in Fig. 4 (a). The plot contour graph shows the response values visualized in blue, green, yellow, and red. The difference in contour color describes the resulting response value differently. Shifting the contour color to blue indicates a lower response value, while a shift to red indicates an increasingly higher response value.

A 3D graph of the response surface between the interaction factors of concentration and power was shown in Fig. 4(b) which forms a parabola facing down. The curve of this 3D response graph corresponds to the results of the quadratic selected model fit summary. The small circular point in the middle of the curve describes the optimum conditions while the brightest point was the maximum condition for the interaction of concentration and power. Based on the graph of the contours of the plot and response surface, the highest degradation efficiency values are in the concentration range of 4%–6% and the power of 480–600 Watt.

Fig. 5 shows a graph of the contours of the plot and the response

Table 5
Analysis of ANOVA response surface quadratic model.

Source	Sum Of Squares	Df	Mean Square	F Value	p-value Prob > F	
Model	2628.56	9	292.06	9.83	0.0007	*Significant*
A-Concentration	628.15	1	628.15	21.15	0.0010	
B-Power	672.90	1	672.90	22.66	0.0008	
C-Time	964.73	1	964.73	32.49	0.0002	
AB	0.22	1	0.22	7.558 E−003	0.9324	
AC	93.85	1	93.85	3.16	0.1058	
BC	9.86	1	9.86	0.33	0.5773	
A^2	194.83	1	194.83	6.56	0.0283	
B^2	329.80	1	329.80	11.11	0.0076	
C^2	107.29	1	107.29	3.61	0.0086	
Residual	296.97	10	29.70			
Lack of fit	83.38	5	16.68	0.39	0.8374	*Not significant*
Pure Error	213.59	5	42.72			
Cor Total	2925.53	19				

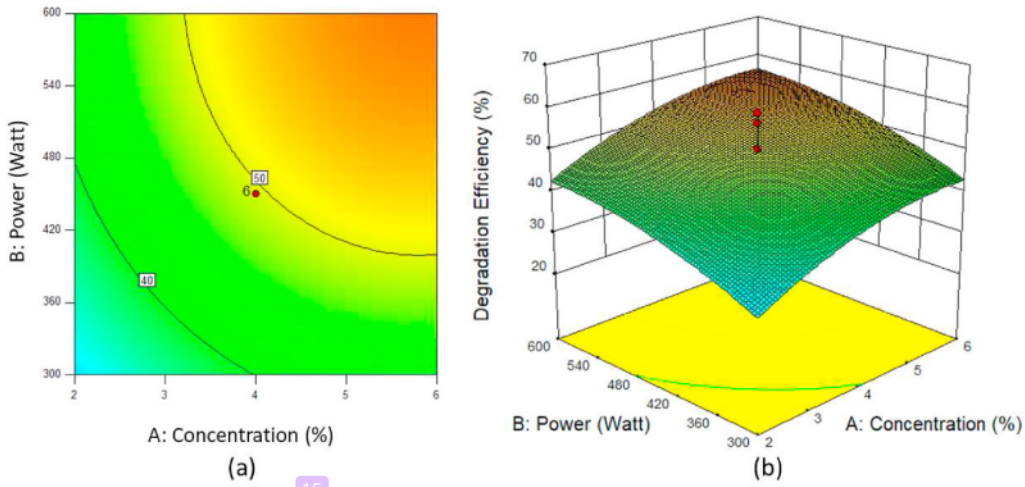

Fig. 4. (a) Contour plot graph (b) 3D Interaction of concentration – power.

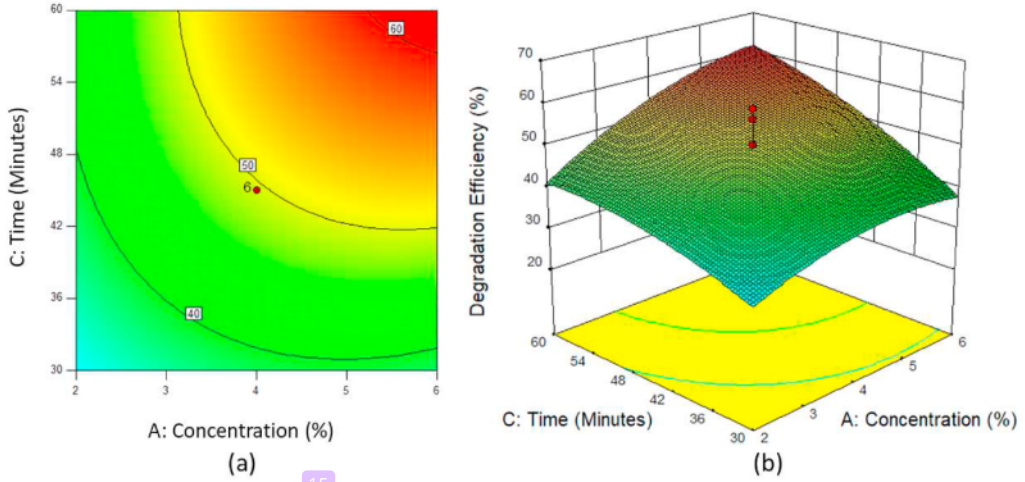

Fig. 5. (a) Contour plot graph (b) 3D Interaction of concentration – time.

surface for the interaction of concentration and time. These color gradation depicted was observed shifting from light blue, green, and yellow toward dark red. The color shift in the contours of this graph indicates the distribution of the resulting degradation efficiency value. A 3D curve of the response surface on this interaction also illustrates the shape of the parabola. Based on the curve, the best conditions for obtaining high degradation efficiency values are generated in the same concentration range of 4%–6% with a time factor of 48 min–60 min.

The interaction between the power and time factors is shown in Fig. 6. The influence of the interaction of these two variables was not much different from the other two interactions. The resulting degradation efficiency value has a distribution of colors that spread from light blue to pink. While the resulting 3D visualization has an arch shape facing down. The best range to produce the best degradation efficiency value in the power range of 480–600 Watts with a synthesis time of 45–60 min.

From the three interactions between variables, it can be known that each factor influences the value of degradation efficiency. The optimum value was generated at concentration conditions between 4% and 6%, power 480 to 600 Watt, and Synthesis time of 45–60 min. A further increase or decrease in each factor has an impact on the low-efficiency value of the resulting degradation.

3.3. Characterization

Characterization of the material was carried out to confirm the successful synthesis of the resulting Bi_2O_3/Cu material. The first test determines the crystallinity of the material with the XRD instrument. The resulting XRD pattern is shown in Fig. 7.

Based on the processing of XRD data obtained the material phase was produced in the form of phase α-Bi_2O_3. These results show that Bi_2O_3 material has actually formed and has an excellent level of stability at low temperatures [47]. The addition of Cu metal material to Bi_2O_3 was also detected in the XRD pattern, namely with the discovery of the Garhadite ($Cu_2H_3NO_6$) phase. The composition of the phases formed are α-Bi_2O_3 by 71.9% and Garhadite by 28.1%. This formed diffraction peak was in accordance with COD (Crystallography Open Database) data numbers 1010004 and 9012715.

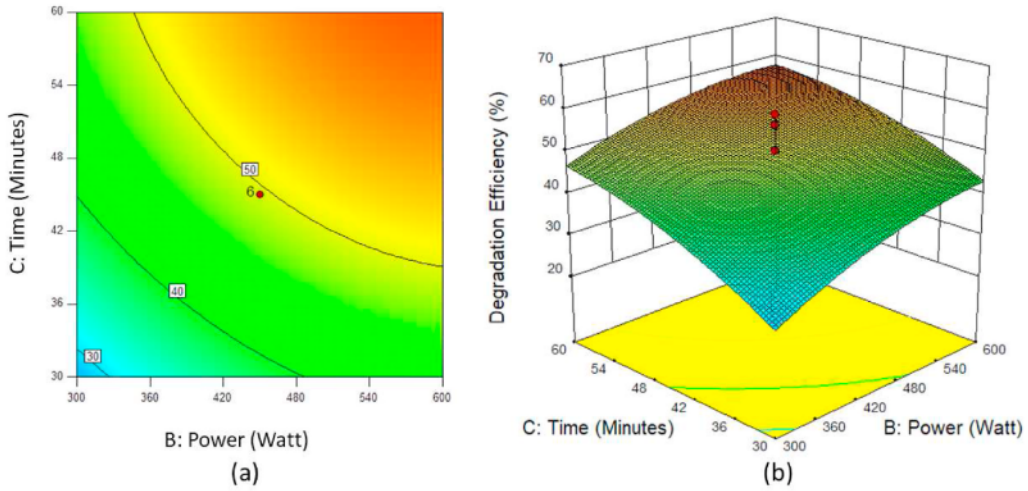

Fig. 6. (a) Contour plot graph (b) 3D Interaction of power – time.

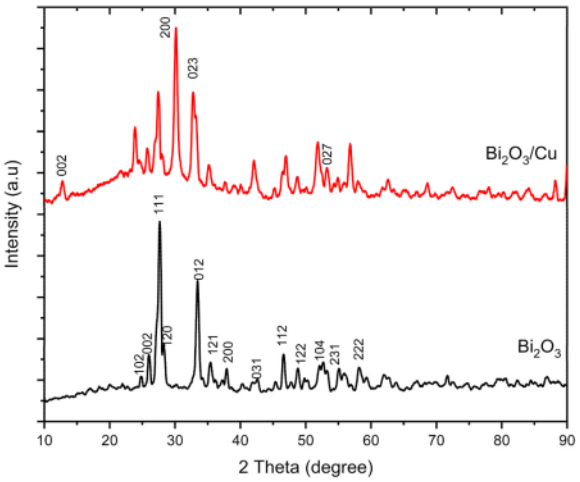

Fig. 7. XRD of Bi_2O_3 and Bi_2O_3/Cu pattern.

Based on calculations using the Debye-Scherrer formula, the resulting Bi_2O_3/Cu crystal size was 31.23874 nm. The size of the crystal is calculated based on the principle of X-ray diffraction, with the distance between the gaps being the distance between atoms in the crystal. The smaller the FWHM value produced, the better the quality of the crystals. This is because the FWHM value indicates that adjacent atoms can adjust the direction and length of their bonds more quickly [48].

The XRD pattern has prominent diffraction peaks, the miller index, FWHM, and phases formed, as shown in the following Table 6.

The resulting Bi_2O_3/Cu energy band gap is shown in Fig. 8. The value of the energy bandgap was obtained from calculations using the Tauc Plot technique which was 2.43 eV. Adding Cu material to Bi_2O_3 resulted in a lower gap value of the resulting energy band. Bi_2O_3 generally has an energy band gap value in the energy band range of 2.58–2.85 [49]. This is evidenced by testing the Bi_2O_3 sample without adding Cu, producing a band gap energy of 2.79 eV.

A reasonably low energy band gap allows Bi_2O_3/Cu to be active in visible light compared to other materials. The low energy band gap will narrow the distance between the valence band and the conduction band.

Table 6
The diffraction peaks, the miller index, FWHM, and phases formed.

2θ (°)	Miller Index	FWHM (rad)	Phase formed
12.77°	002	0.28777	Garhardite ($Cu_2H_3NO_6$)
24.63°	102	0.2636	α-Bi_2O_3
25.87°	002	0.2636	α-Bi_2O_3
27.04°	111	0.2636	α-Bi_2O_3
27.52°	120	0.2636	α-Bi_2O_3
28.13°	012	0.2636	α-Bi_2O_3
32.75°	200	0.28777	Garhardite ($Cu_2H_3NO_6$)
33.19°	121	0.2636	α-Bi_2O_3
33.29°	200	0.2636	α-Bi_2O_3
35.15°	023	0.28777	Garhardite ($Cu_2H_3NO_6$)
35.48°	031	0.2636	α-Bi_2O_3
37.64°	112	0.2636	α-Bi_2O_3
42.42°	122	0.2636	α-Bi_2O_3
48.67°	104	0.2636	α-Bi_2O_3
53.07°	231	0.2636	α-Bi_2O_3
54.88°	027	0.28777	Garhardite ($Cu_2H_3NO_6$)
55.68°	222	0.2636	α-Bi_2O_3

As a result, when excitation occurs due to the release of photon energy during UV light irradiation, it will increase the production of electrons and holes. It shows the energy required by the electron to move from the valence band to the conduction band gets smaller. The higher production of electrons and holes can increase the photocatalytic activity of materials.

The resulting morphology of Bi_2O_3/Cu can be known by SEM analysis as shown in Fig. 9. Pure particles of Bi_2O_3/Cu are indicated by the shape of a rod as shown in Fig. 9(a) similar with the Ravele et.al research report [48]. Rod-shaped particles are scattered around spherical particles. This particle with a dominant round shape was a Cu particle that was added with a concentration of 6%. The addition of Cu with a high concentration resulted in a number of spherical particles having a large size. These results increase the efficiency of TC degradation because Cu particles entering the Bi_2O_3/Cu matrix can inhibit recombination so that photocatalytic activity will be maximized [49].

The particle size was calculated using ImageJ software. The average particle size of Bi_2O_3/Cu produced was 1.3503 μm. The measured particle size of the SEM image has a larger size than the crystallite size of the XRD calculation. This is because the particles produced are grouped, which causes agglomeration during synthesis. The structure of Cu particles, which resemble porous spheres, can increase the photocatalytic

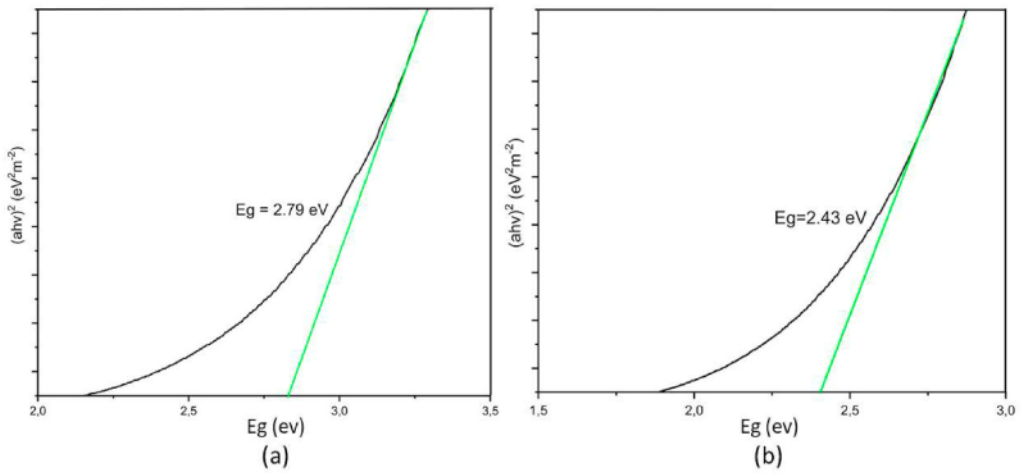

Fig. 8. (a). Energy bandgap of Bi_2O_3 and (b) Energy band gap of Bi_2O_3/Cu.

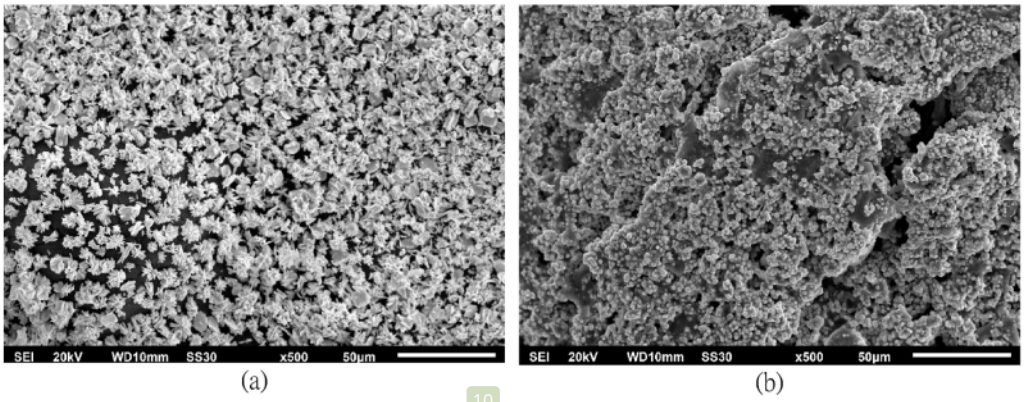

Fig. 9. SEM image of (a) Bi_2O_3, and (b) Bi_2O_3/Cu.

activity of the material. One of the requirements for a good photocatalyst material is to have a porous surface to increase the surface area for photon absorption during photocatalysis. A large surface area results in more vacancies, thereby increasing the diffusion between TC pollutant molecules and photocatalyst materials.

The discovery of Bi and Cu particles in SEM results was confirmed through the EDX results shown in Table 7.

TC Degradation Mechanism using Bi_2O_3/Cu.

The degradation of TC can be known based on the photocatalytic activity of Bi_2O_3/Cu. Photocatalytic activity indicates a continuous decrease in absorption, efficiency value, and degradation rate. This decrease in the level of degradation occurs due to the presence of irradiation with UV rays. Compared to the adsorption process, the photocatalytic process is superior because the process is continuous. This can be seen in Fig. 10 (a) which indicates a decrease in the absorbance value of TC along with the length of irradiation time, indicating that the photocatalytic process is continuously continuous. The longer the irradiation time, the more degraded TC will increase. This is evidenced by the increase in the value of degradation efficiency along with the length of time of irradiation as seen in Fig. 10 (b).

Table 7
Result of SEM-EDX

Element	Mass (%)	Sigma	Atom (%)
O	0.525	0.33	86.45
Cu	8.040	0.14	0.98
Bi	2.419	0.54	12.57

Fig. 11 shown the TC degradation mechanism by Bi_2O_3/Cu photocatalyst material. Its occurs when the material was irradiated with UV light that has the same photon energy ($E = h\nu$) or greater than the energy of the bandgap ($h\nu \geq Eg$). Absorption of photons caused excitation and transfer of electrons (e^-) from the valence band to the conduction band. Separation and migration of load carriers (e^- and h^+) to the surface occur material. Highly reactive electrons and holes in the photocatalyst surface. It tends to perform reduction and oxidation reactions to produce hydroxyl radicals ($\bullet OH^-$) and superoxide radicals ($\bullet O_2^-$) respectively. The photodegradation process of Bi_2O_3/Cu photocatalyst material was indicated through the following reaction:

$$Bi_2O_3 + h\nu \rightarrow e^- + h^+ \quad (1)$$

$$O_2 + Bi_2O_3(e^-CB) \rightarrow O_2^- \quad (2)$$

The absorption of photon energy causes the rise of electrons from the valence band to the conduction band. The resulting hole was responsible for the formation of hydroxyl radicals that will attach to the

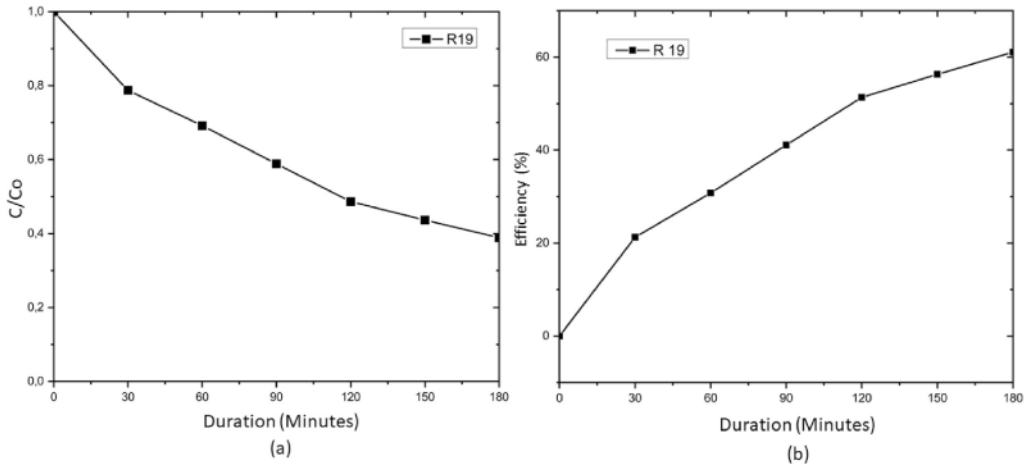

Fig. 10. TC degradation mechanism using Bi_2O_3/Cu.

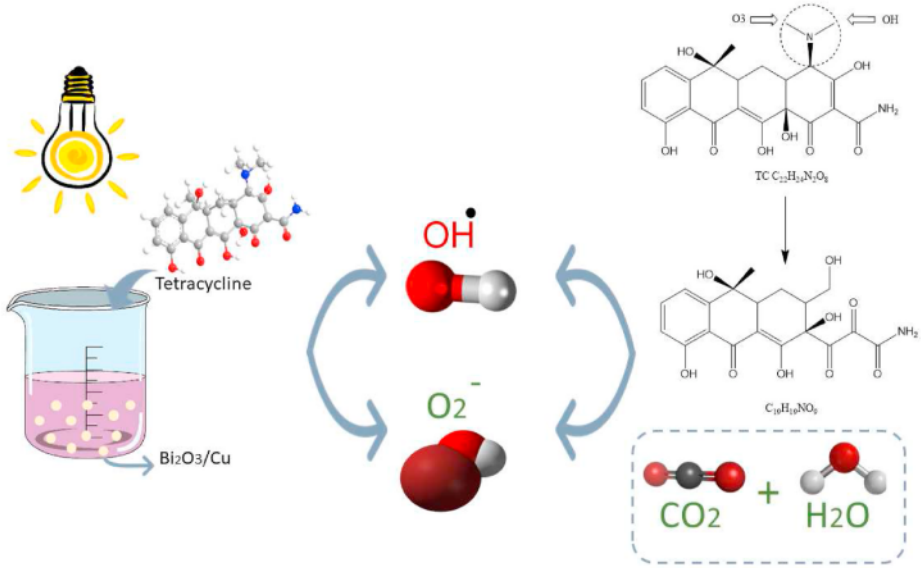

Fig. 11. Mechanism of tetracycline degradation by Bi_2O_3/Cu.

photocatalyst surface. In the photocatalyst process, the separation and recombination of the load carrier light-induced will occur quickly. Once the electron moves from the valence band it will return to the conduction band [44]. Effective photocatalyst activity occurs when recombination between two load carriers was prevented by the proving of Cu doping.

$$Cu^{+} + h^{+} \rightarrow Cu^{2+} \quad (3)$$

$$Cu^{+} + e^{-} \rightarrow Cu \quad (4)$$

$$Cu^{2+} + O_2(ads) \rightarrow Cu^{3+} + O_2^{-} \quad (5)$$

$$Cu + OH^{-}(ads) \rightarrow Cu + OH^{-}(ads) \quad (6)$$

Cu^{+} ions inserted into the photocatalyst material matrix absorb electrons that have been excited by photons and turn into Cu^{2+} ions. These ions react with the O_2 molecule and produce superoxide ($\bullet O2^{-}$) and Cu^{3+} radical ions that act as electron collectors. This will lead to the occurrence of recombination stability and increased photocatalyst activity in the material [46].

12

$$O_2^{-} + H^{+} \rightarrow OOH \quad (7)$$

$$O_2^{-} + H^{+} + OOOH \rightarrow H_2O_2 + O_2 \quad (8)$$

$$H_2O_2 + O_2^{-} \rightarrow OH + OH^{-} + O_2 \quad (9)$$

$$TC^{+} + \left(OH,\ O_2^{-} + O_2\right) \rightarrow CO_2 + H_2O + \text{organic compounds} \quad (10)$$

$$h^{+}TC \rightarrow CO_2 + H_2O + \text{organic compounds} \quad (11)$$

The degradation process occurs through the transfer of charge from the charge carriers, namely hydroxyl radicals and superoxide radicals

that serve as oxidizing agents and decreasing TC compounds. These two charge carriers will form CO_2, H_2O, and other inorganic components. This reaction will bind TC pollutants around the Bi_2O_3/Cu material as long as the material is irradiated by UV light so that it can lower TC and TC pollutants can be degraded.

Excess Cu^{3+} ions will enter the cluster. These clusters can withstand TC photodegradation by covering the active site from the Bi_2O_3 surface. Cu^{3+} ions will act as photons generated between the hole and electron transfer. The recombination rate during irradiation can be suppressed by increasing the amount trapped by the electron to increase the electron and hole service life. The final result of the photodegradation process is TC, degraded and organic materials in the form of CO_2 and H_2O.

This decrease in the level of recombination increases the photocatalytic activity of Bi_2O_3/Cu. To degrade under sunlight irradiation, it is necessary to modify the energy band gap of the Bi_2O_3/Cu material according to the energy of the visible light band gap. In this study, researchers have modified the energy band gap to 2.43 eV so that, in principle, it is possible to transfer electrons, and photocatalytic reactions will occur in sunlight.

4. Conclusion

The synthesis of Bi_2O_3/Cu has been successfully carried out using the microwave-assisted precipitation method. Optimization was carried out on 3 factors namely concentration, power, and synthesis time with the best response obtained at R19 with a combination of 6% concentration, 600 W of power, and 60 min of time, respectively. Bi_2O_3/Cu material is able to degrade Tetracycline with a degradation percentage value of 61.09%.

Credit author statement

Fatkhiyatus Sa'adah: Conceptualization, Methodology, Investigation. **Heri Sutanto**: Formal Analysis, Data Validation. **Hadiyanto**: Writing- Reviewing and Editing.

Declaration of competing interest

The authors declare that they have no known competing financial interests or personal relationships that could have appeared to influence the work reported in this paper.

Acknowledgment

This work was supported by The Ministry of Education, Culture, Research, and Technology of Republic Indonesia by PMDSU Batch VI Scheme with contract no.: 345-41/UN7.6.1/PP/2022.

References

[1] E. Méndez, M.A. González-Fuentes, G. Rebollar-Perez, A. Méndez-Albores, E. Torres, Emerging pollutant treatments in wastewater: cases of antibiotics and hormones [Internet], J Environ Sci Heal - Part A Toxic/Hazardous Subst Environ Eng 52 (3) (2017) 235–253. Available from: https://www.tandfonline.com/doi/abs/10.1080/10934529.2016.1253391.

[2] J. Wang, S. Wang, Removal of pharmaceuticals and personal care products (PPCPs) from wastewater: a review [Internet], J. Environ. Manag. 182 (2016) 620–640. Available from: https://api.elsevier.com/content/article/eid/1-s2.0-S0301479716304868.

[3] M. Tanveer, G.T. Guyer, G. Abbas, Photocatalytic degradation of ibuprofen in water using TiO_2 and ZnO under artificial UV and solar irradiation [Internet], Water Environ Res 91 (9) (2019 Sep 8) 822–829. Available from: https://onlinelibrary.wiley.com/doi/abs/10.1002/wer.1104.

[4] J. Wang, R. Zhuan, L. Chu, The occurrence, distribution and degradation of antibiotics by ionizing radiation: an overview [Internet], Sci Total Environ 646 (2019) 1385–1397, https://doi.org/10.1016/j.scitotenv.2018.07.415. Available from:.

[5] S. Wang, J. Wang, Degradation of carbamazepine by radiation-induced activation of peroxymonosulfate [Internet], Chem Eng J 336 (2018) 595–601, https://doi.org/10.1016/j.cej.2017.12.068 (October 2017), Available from:.

[6] M. Östman, R.H. Lindberg, J. Fick, E. Björn, M. Tysklind [Internet], Screening of Biocides, Metals and Antibiotics in Swedish Sewage Sludge and Wastewater, vol. 115, Water Res, 2017, pp. 318–328. Available from: doi:10.1016/j.watres.2017.03.011..

[8] T. Yang, J. Peng, Y. Zheng, X. He, Y. Hou, L. Wu, et al., Enhanced photocatalytic ozonation degradation of organic pollutants by ZnO modified TiO_2 nanocomposites [Internet], Appl Catal B Environ 221 (2018) 223–234. Available from: https://api.elsevier.com/content/article/eid/1-s2.0-S0926337317308640.

[9] J. Ding, Z. Dai, F. Qin, H. Zhao, S. Zhao, R. Chen, Z-scheme $BiO_{1-x}Br$/$Bi_2O_2CO_3$photocatalyst with rich oxygen vacancy as electron mediator for highly efficient degradation of antibiotics [Internet], Appl. Catal. B Environ. 205 (2017) 281–291. Available from: https://api.elsevier.com/content/article/eid/1-s2.0-S0926337316309493.

[10] R. Kafaei, F. Papari, M. Seyedabadi, S. Sahebi, R. Tahmasebi, M. Ahmadi, et al., Occurrence, distribution, and potential sources of antibiotics pollution in the water-sediment of the northern coastline of the Persian Gulf, Iran [Internet], Sci. Total Environ. 627 (2018) 703. –12. Available from: https://api.elsevier.com/content/article/eid/1-s2.0-S0048969718303474.

[11] M. Pan, L.M. Chu, Occurrence of antibiotics and antibiotic resistance genes in soils from wastewater irrigation areas in the Pearl River Delta region, southern China [Internet], Sci. Total Environ. 624 (2018) 145–152, https://doi.org/10.1016/j.scitotenv.2017.12.008. Available from:.

[12] T.X. Wang, H.P. Liang, D.A. Anito, X. Ding, B.H. Han, Emerging applications of porous organic polymers in visible-light photocatalysis [Internet], J. Mater. Chem. 8 (15) (2020) 7003. –34. Available from: https://pubs.rsc.org/en/content/articlehtml/2020/ta/d0ta00364f.

[13] T.H. Grossman, Tetracycline antibiotics and resistance, Cold Spring Harb Perspect Med 6 (4) (2016).

[14] P.H. Chang, Z. Li, J.S. Jean, W.T. Jiang, Q. Wu, C.Y. Kuo, et al., Desorption of tetracycline from montmorillonite by aluminum, calcium, and sodium: an indication of intercalation stability, Int. J. Environ. Sci. Technol. 11 (3) (2014) 633–644.

[15] G.H. Safari, M. Hoseini, M. Seyedsalehi, H. Kamani, J. Jaafari, A.H. Mahvi, Photocatalytic degradation of tetracycline using nanosized titanium dioxide in aqueous solution [Internet], Int J Environ Sci Technol 12 (2) (2015) 603–616. Available from: https://link.springer.com/content/pdf/10.1007/s13762-014-0706-9.pdf.

[16] N. Czekalski, T. Berthold, S. Caucci, A. Egli, H. Bürgmann, Increased levels of multiresistant bacteria and resistance genes after wastewater treatment and their dissemination into Lake Geneva, Switzerland, Front. Microbiol. 3 (MAR) (2012) 1–18.

[17] X. Zhang, W. Guo, H.H. Ngo, H. Wen, N. Li, W. Wu, Performance evaluation of powdered activated carbon for removing 28 types of antibiotics from water [Internet], J Environ Manage 172 (2016) 193–200, https://doi.org/10.1016/j.jenvman.2016.02.038. Available from:.

[18] T. Saitoh, K. Shibata, K. Fujimori, Y. Ohtani, Rapid removal of tetracycline antibiotics from water by coagulation-flotation of sodium dodecyl sulfate and poly (allylamine hydrochloride) in the presence of Al(III) ions [Internet], Separ. Purif. Technol. 187 (Iii) (2017) 76–83, https://doi.org/10.1016/j.seppur.2017.06.036. Available from:.

[19] I. Senta, S. Terzic, M. Ahel, Occurrence and fate of dissolved and particulate antimicrobials in municipal wastewater treatment [Internet], Water Res 47 (2) (2013) 705–714, https://doi.org/10.1016/j.watres.2012.10.041. Available from:.

[20] L. Feng, M.E. Casas, L.D.M. Ottosen, H.B. Møller, K. Bester, Removal of antibiotics during the anaerobic digestion of pig manure [Internet], Sci. Total Environ. 603 (2017), https://doi.org/10.1016/j.scitotenv.2017.05.280. –604:219–25. Available from:.

[21] E. Shang, Y. Li, J. Niu, S. Li, G. Zhang, X. Wang, Photocatalytic degradation of perfluorooctanoic acid over Pb-$BiFeO_3$/rGO catalyst: kinetics and mechanism [Internet], Chemosphere 211 (2018) 34–43. Available from: https://api.elsevier.com/content/article/eid/1-s2.0-S0045653518313997.

[22] Y. Yang, X. Li, C. Zhou, W. Xiong, G. Zeng, D. Huang, et al. [Internet], Recent advances in application of graphitic carbon nitride-based catalysts for degrading organic contaminants in water through advanced oxidation processes beyond photocatalysis: A critical review, vol. 184, Water Research, 2020. Available from: https://api.elsevier.com/content/article/eid/1-s2.0-S0043135420307375.

[23] Y.M. Hunge, A.A. Yadav, S.W. Kang, H. Kim, Photocatalytic degradation of tetracycline antibiotics using hydrothermally synthesized two-dimensional molybdenum disulfide/titanium dioxide composites, J. Colloid Interface Sci. 606 (2022) 454–463.

[24] S. Li, Z. Wang, X. Zhao, X. Yang, G. Liang, X. Xie [Internet], Insight into enhanced carbamazepine photodegradation over biochar-based magnetic photocatalyst Fe3O4/BiOBr/BC under Visible LED Light Irradiation, vol. 360, Chemical Engineering Journal. Elsevier, 2019, p. 600, 11. Available from: https://www.sciencedirect.com/science/article/pii/S1385894718324744.

[25] E. Márquez Brazón, C. Piccirillo, I.S. Moreira, P.M.L. Castro [Internet], Photodegradation of pharmaceutical persistent pollutants using hydroxyapatite-based materials, vol. 182, Journal of Environmental Management. Elsevier, 2016, pp. 486–495. Available from: https://www.sciencedirect.com/science/article/pii/S0301479716305424.

[26] M.G. Dong, M.I. Sayyed, G. Lakshminarayana, M. Çelikbilek Ersundu, A. E. Ersundu, P. Nayar, et al., Investigation of gamma radiation shielding properties of lithium zinc bismuth borate glasses using XCOM program and MCNP5 code [Internet], J. Non-Cryst. Solids 468 (2017) 12–16. Available from: https://api.elsevier.com/content/article/eid/1-s2.0-S0022309317301941.

[27] A.C. Martins, A.L. Cazetta, O. Pezoti, J.R.B. Souza, T. Zhang, E.J. Pilau, et al., Sol-gel synthesis of new TiO_2/activated carbon photocatalyst and its application for degradation of tetracycline [Internet], Ceram Int 43 (5) (2017) 4411–4418. Available from: https://www.sciencedirect.com/science/article/pii/S0272884216323550.

[28] L. Rimoldi, D. Meroni, G. Cappelletti, S. Ardizzone, Catal Today [Internet], Green and low cost tetracycline degradation processes by nanometric and immobilized TiO2 systems, vol. 281, Elsevier, 2017, pp. 38–44. Available from: https://www.sciencedirect.com/science/article/pii/S092058611630520X.

[29] K.P. Priyanka, S. Sankararaman, K.M. Balakrishna, T. Varghese, Enhanced visible light photocatalysis using TiO_2/phthalocyanine nanocomposites for the degradation of selected industrial dyes [Internet], J Alloys Compd 720 (2017) 541–549, https://doi.org/10.1016/j.jallcom.2017.05.308. Available from:.

[30] Y. Yan, Z. Zhou, Y. Cheng, L. Qiu, C. Gao, J. Zhou, Template-free fabrication of α- and β-Bi_2O_3 hollow spheres and their visible light photocatalytic activity for water purification [Internet], J Alloys Compd 605 (2014) 102–108, https://doi.org/10.1016/j.jallcom.2014.03.111. Available from:.

[31] Z. Ai, S. Lee, Morphology-dependent photocatalytic removal of NO by hierarchical BiVO 4 microboats and microspheres under visible light [Internet], Appl Surf Sci 280 (2013) 354–359, https://doi.org/10.1016/j.apsusc.2013.04.160. Available from:.

[32] S. Sharma, A.O. Ibhadon, M. Grazia Francesconi, S.K. Mehta, S. Elumalai, S. K. Kansal, et al., Bi_2WO_6/C-dots/TiO_2: a novel z-scheme photocatalyst for the degradation of fluoroquinolone levofloxacin from aqueous medium [Internet], Nanomaterials 10 (5) (2020). Available from: https://www.mdpi.com/711210.

[33] L. Zhang, C. Baumanis, L. Robben, T. Kandiel, D. Bahnemann, Bi_2WO_6 inverse opals: facile fabrication and efficient visible-light-driven photocatalytic and photoelectrochemical water-splitting activity [Internet], Small 7 (19) (2011 Oct 4) 2714–2720. Available from: https://onlinelibrary.wiley.com/doi/10.1002/smll.201101152.

[34] Z. Wei, J. Liu, W. Shangguan, A review on photocatalysis in antibiotic wastewater: pollutant degradation and hydrogen production [Internet], Chinese J Catal 41 (10) (2020 Oct) 1440–1450. Available from: https://www.sciencedirect.com/science/article/pii/S1872206719634480.

[35] M. Yang, Q. Yang, J. Zhong, S. Huang, J. Li, J. Song, et al., Enhanced photocatalytic performance of Ag_2O/BiOF composite photocatalysts originating from efficient interfacial charge separation [Internet], Appl Surf Sci 416 (2017) 666–671. Available from: https://api.elsevier.com/content/article/eid/1-s2.0-S0169433217312424.

[36] G. Liu, S. Li, Y. Lu, J. Zhang, Z. Feng, C. Li, Controllable synthesis of α-$Bi_2O_3$and γ-$Bi_2O_3$with high photocatalytic activity by α-Bi_2O_3→γ-Bi_2O_3→α-Bi_2O_3transformation in a facile precipitation method, J. Alloys Compd. 689 (2016) 787–799.

[37] Z.A. Zulkifli, K.A. Razak, W.N.W.A. Rahman, S.Z. Abidin, Synthesis and characterisation of bismuth oxide nanoparticles using hydrothermal method: the effect of reactant concentrations and application in radiotherapy [internet], in: Journal of Physics: Conference Series, vol. 1082IOP Publishing, 2018. Available from: https://iopscience.iop.org/article/10.1088/1742-6596/1082/1/012103.

[38] G. Zhu, W. Que, J. Zhang, Synthesis and photocatalytic performance of Ag-loaded β-Bi_2O_3 microspheres under visible light irradiation [Internet], J Alloys Compd 509 (39) (2011) 9479–9486, https://doi.org/10.1016/j.jallcom.2011.07.046. Available from:.

[39] Y. Astuti, A. Arnelli, P. Pardoyo, A. Fauziyah, S. Nurhayati, A.D. Wulansari, et al., Studying impact of different precipitating agents on crystal structure, morphology, and photocatalytic activity of bismuth oxide, Bull Chem React Eng & Catal 12 (3) (2017) 478, 84.

[40] Y. Huang, D. Ding, M. Zhu, W. Meng, Y. Huang, F. Geng, et al., Facile synthesis of α-Fe_2O_3 nanodisk with superior photocatalytic performance and mechanism insight [Internet], in: Science and Technology of Advanced Materials, vol. 16Taylor & Francis, 2015. Available from: https://www.tandfonline.com/doi/full/10.1088/1468-6996/16/1/014801.

[41] Y. Xie, C. Zhang, D. Wang, J. Lu, Y. Wang, J. Wang, et al., Catalytic performance of a Bi_2O_3-Fe_2O_3 system in soot combustion, New J. Chem. 43 (38) (2019) 15368–15374.

[42] T. Prakoso, I.B. Kurniawan, R.H. Nugroho, Esterification of free fatty acid, Jurnal Teknik Kimia Indonesia, 2018, pp. 705–709.

[43] A.G. Khosroshahi, A. Mehrizad, Optimization, kinetics and thermodynamics of photocatalytic degradation of Acid Red 1 by Sm-doped CdS under visible light [Internet], Journal of Molecular Liquids. Elsevier 275 (2019) 629–637. Available from: https://www.sciencedirect.com/science/article/pii/S0167732218338467.

[44] H. Hadiyanto, M. Christwardana, W.Z. Pratiwi, P. Purwanto, S. Sudarno, K. Haryani, et al., Response surface optimization of microalgae microbial fuel cell (MMFC) enhanced by yeast immobilization for bioelectricity production [Internet], Chemosphere 287 (P3) (2022), 132275, https://doi.org/10.1016/j.chemosphere.2021.132275. Available from:.

[45] J. Kabuba, M. Banza, Ion-exchange process for the removal of Ni (II) and Co (II) from wastewater using modified clinoptilolite: modeling by response surface methodology and artificial neural network [Internet], Results Eng 8 (November) (2020), 100189, https://doi.org/10.1016/j.rineng.2020.100189. Available from:.

[46] I. Alkian, H. Sutanto, H. Hadiyanto, Quantum yield optimization of carbon dots using response surface methodology and its application as control of Fe^{3+}ion levels in drinking water, Mater. Res. Express 9 (1) (2022), https://doi.org/10.1088/2053-1591/ac3f60.

[47] J. Chen, X.D. Wei, Y.S. Liu, G.G. Ying, S.S. Liu, L.Y. He, et al., Removal of antibiotics and antibiotic resistance genes from domestic sewage by constructed wetlands: optimization of wetland substrates and hydraulic loading [Internet], Sci. Total Environ. 565 (2016) 240. –8. Available from: https://api.elsevier.com/content/article/eid/1-s2.0-S0048969716308786.

[48] M.P. Ravele, O.A. Oyewo, S. Ramaila, L. Mavuru, D.C. Onwudiwe, Facile synthesis of copper oxide nanoparticles and their applications in the photocatalytic degradation of acyclovir, Results Eng [Internet] vol. 14, Elsevier, 2022. Available from: https://www.sciencedirect.com/science/article/pii/S2590123022001499.

[49] H. Sutanto, E. Hidayanto, M. Mukholit, S. Wibowo, I. Nurhasanah, H. Hadiyanto, The physical and photocatalytic properties of N-doped TiO_2 polycrystalline synthesized by a single step sonochemical method at room temperature, Mater. Sci. Forum 890 (2017) 121–126, https://doi.org/10.4028/www.scientific.net/MSF.890.121.

Further Reading

[7] J. Fick, H. Söderström, R.H. Lindberg, C. Phan, M. Tysklind, D.G.J. Larsson, Contamination of surface, ground, and drinking water from pharmaceutical production, Environ. Toxicol. Chem. vol. 28 (12) (2009) 2522–2527, https://doi.org/10.1897/09-073.1.

51. Optimzition of the Bi2O3Cu synthesis process using response surface methodology as a tetracycline photodegradation agent

ORIGINALITY REPORT

10%	8%	6%	4%
SIMILARITY INDEX	INTERNET SOURCES	PUBLICATIONS	STUDENT PAPERS

PRIMARY SOURCES

1	www.mdpi.com Internet Source	1%
2	Changyu Lu, Daiqiong Yang, Lantao Wang, Sijie Wen, Delu Cao, Chengqi Tu, Luning Gao, Yuliang Li, Yahong Zhou, Wei Huang. "Facile construction of CoO/Bi2WO6 p-n heterojunction with following Z-Scheme pathways for simultaneous elimination of tetracycline and Cr(VI) under visible light irradiation", Journal of Alloys and Compounds, 2022 Publication	1%
3	www.researchgate.net Internet Source	1%
4	repository.upstegal.ac.id Internet Source	<1%
5	M Hapsari, A H Cahyana, R T Yunarti. " One-pot synthesis of spirooxindole-pyrrolizidine compounds using magnetically separable Fe	<1%

	O -graphene oxide (Fe O -GO) catalyst ", IOP Conference Series: Materials Science and Engineering, 2020 Publication	
6	Submitted to King's College Student Paper	<1 %
7	vital.seals.ac.za:8080 Internet Source	<1 %
8	link.springer.com Internet Source	<1 %
9	Reenamole Georgekutty, Michael K. Seery, Suresh C. Pillai. "A Highly Efficient Ag-ZnO Photocatalyst: Synthesis, Properties, and Mechanism", The Journal of Physical Chemistry C, 2008 Publication	<1 %
10	pubs.rsc.org Internet Source	<1 %
11	Submitted to Durban University of Technology Student Paper	<1 %
12	Submitted to Indian Institute of Technology, Bombay Student Paper	<1 %
13	ijpsr.com Internet Source	<1 %

14	jmrt.com.br Internet Source	<1 %
15	Submitted to Universiti Malaysia Pahang Student Paper	<1 %
16	Submitted to Universiti Malaysia Perlis Student Paper	<1 %
17	Submitted to Lincoln Park High School Student Paper	<1 %
18	open.uct.ac.za Internet Source	<1 %
19	G. H. Safari, M. Hoseini, M. Seyedsalehi, H. Kamani, J. Jaafari, A. H. Mahvi. "Photocatalytic degradation of tetracycline using nanosized titanium dioxide in aqueous solution", International Journal of Environmental Science and Technology, 2014 Publication	<1 %
20	www.degruyter.com Internet Source	<1 %
21	comptes-rendus.academie-sciences.fr Internet Source	<1 %
22	www.akamaiuniversity.us Internet Source	<1 %
23	Submitted to Asian Institute of Technology Student Paper	<1 %

24	cyberleninka.org Internet Source	<1 %
25	moam.info Internet Source	<1 %
26	unsworks.unsw.edu.au Internet Source	<1 %
27	www.scipress.com Internet Source	<1 %
28	Zhang, Gaoke, Qiao Xiong, Wei Xu, and Sheng Guo. "Synthesis of bicrystalline TiO2 supported sepiolite fibers and their photocatalytic activity for degradation of gaseous formaldehyde", Applied Clay Science, 2014. Publication	<1 %
29	dokumen.pub Internet Source	<1 %
30	ebin.pub Internet Source	<1 %
31	espace.curtin.edu.au Internet Source	<1 %
32	s3-ap-southeast-1.amazonaws.com Internet Source	<1 %
33	Akashdeep Singh Oberoi, Yanyan Jia, Huiqun Zhang, Samir Kumar Khanal, Hui Lu. "Insights	<1 %

into the Fate and Removal of Antibiotics in Engineered Biological Treatment Systems: A Critical Review", Environmental Science & Technology, 2019
Publication

34	Armando Jorge Monteiro Neves Padilha and João Manuel Ribeiro da Silva Tavares. "Algumas ferramentas para visão tridimensional por computador", Repositório Aberto da Universidade do Porto, 2011. Publication	<1 %
35	Nanostructure Science and Technology, 2016. Publication	<1 %
36	downloads.hindawi.com Internet Source	<1 %
37	etheses.uin-malang.ac.id Internet Source	<1 %
38	pdfcoffee.com Internet Source	<1 %
39	repository.up.ac.za Internet Source	<1 %
40	tud.qucosa.de Internet Source	<1 %
41	www.ajol.info Internet Source	<1 %

www.cambridge.org

42	Internet Source	<1%
43	www.drmgrdu.ac.in Internet Source	<1%
44	www.science.gov Internet Source	<1%

Exclude quotes	Off	Exclude matches	Off
Exclude bibliography	On		